Coherent control of attosecond emission from aligned molecules

W. BOUTU[1], S. HAESSLER[1], H. MERDJI[1], P. BREGER[1], G. WATERS[2], M. STANKIEWICZ[3], L. J. FRASINSKI[4], R. TAIEB[5,6], J. CAILLAT[5,6], A. MAQUET[5,6], P. MONCHICOURT[1], B. CARRE[1] AND P. SALIERES[1]*

[1]CEA-Saclay, DSM, Service des Photons, Atomes et Molécules, 91191 Gif sur Yvette, France
[2]J.J. Thomson Physical Laboratory, University of Reading, Whiteknights, Reading RG6 6AF, UK
[3]Institute of Physics, Jagiellonian University, ul. Reymonta 4, 30-059 Kraków, Poland
[4]The Blackett Laboratory, Imperial College London, Prince Consort Road, London SW7 2BW, UK
[5]UPMC Univ Paris 06, UMR 7614, Laboratoire de Chimie Physique-Matière et Rayonnement, 11 rue Pierre et Marie Curie, 75231 Paris Cedex 05, France
[6]CNRS, UMR 7614, LCPMR F-75005 Paris, France
*e-mail: pascal.salieres@cea.fr

Published online: 4 May 2008; doi:10.1038/nphys964

Controlling attosecond electron wave packets and soft X-ray pulses represents a formidable challenge of general implication to many areas of science[1–4]. A strong laser field interacting with atoms or molecules drives ultrafast intra-atomic/molecular electron wave packets on a subfemtosecond timescale, resulting in the emission of attosecond bursts of extreme-ultraviolet light[5,6]. Controlling the intra-atomic/molecular electron dynamics enables steering of the attosecond emission[7,8]. Here, we carry out a coherent control in linear molecules, where the interaction of the laser-driven electron wave packet with the core leads to quantum interferences[9–12]. We demonstrate that these interferences can be finely controlled by turning the molecular axis relative to the laser polarization, that is, changing the electron recollision angle. The wave-packet coulombic distortion modifies the spectral phase jump measured in the extreme-ultraviolet emission. Our attosecond control of the interference results in attosecond pulse shaping, useful for future applications in ultrafast coherent control of atomic and molecular processes.

High harmonic generation in gases[13,14] is a spectacular process arising when a strong laser field tunnel ionizes an atom/molecule, creating an attosecond electron wave packet that is subsequently accelerated and driven back to the core by the laser field[15,16]. It may then recombine to the ground state, releasing its accumulated kinetic energy in the form of an attosecond burst of extreme-ultraviolet light. In a multicycle laser field, this process is repeated every half-cycle leading to a train of attosecond pulses, the spectrum of which contains only the odd harmonics of the laser frequency. The precise characterization of this attosecond emission gives insight into the ultrafast electron dynamics[17]. A control of the continuum electron dynamics—and of the resulting extreme-ultraviolet emission—can be carried out by shaping the laser field, through a time-varying polarization[7] or a multicolour superposition[8]. Our approach is to coherently control the recombination step in linear molecules, when the returning electron wave packet interacts with the multicentre core, leading to quantum interferences[9–12].

A simple way to describe such interferences in diatomic molecules is the two-centre interference model[9,18]: the recolliding electron wave packet is modelled by a plane wave $\Psi_c \propto \exp[i\mathbf{kr}]$, and the ground state (the highest occupied molecular orbital, HOMO) by a linear combination of atomic orbitals. For an antisymmetric combination: $\Psi_0 \propto \Phi_0(\mathbf{r}-\mathbf{R}/2) - \Phi_0(\mathbf{r}+\mathbf{R}/2)$, where $\mathbf{R}$ is the internuclear vector, the recombination dipole moment in the velocity form[19] reads:

$$\langle \Psi_c|\mathbf{p}|\Psi_0\rangle \propto i\mathbf{k}\sin(\mathbf{kR}/2)\langle \exp[i\mathbf{kr}]|\Phi_0\rangle, \quad (1)$$

where $\mathbf{p}$ is the dipole momentum operator.

A destructive interference is obtained at $\mathbf{kR}/2 = n\pi$, that is, when

$$R\cos\theta = n\lambda_e, \quad (2)$$

where θ is the angle between the molecular axis and the electron propagation direction given by the laser polarization, n is an integer and λ_e is the electron de Broglie wavelength. The molecule then behaves like a two-point emitter, the emissions of which are dephased owing to the path difference between the centres and the symmetry of the orbital.

The CO_2 molecule, although triatomic, provides good conditions for observing this quantum interference. Indeed, its HOMO is a Π orbital dominated by the antisymmetric combination of two p orbitals centred on the O atoms. Moreover, the O–O distance ($R_{O-O} = 4.39$ a.u.) corresponds to an electron wavelength typical of the harmonic generation process. The recombination dipole moment exhibits a clear minimum close to that expected from equation (2)—however, for $R = 3.9$ a.u. $< R_{O-O}$ (Fig. 1). This deviation is due to a non-negligible contribution to the HOMO from the d_{xy} carbon orbital, and also to a lesser extent from the d_{xy} oxygen orbitals, the symmetry of which does not correspond to the interference condition (2).

The electron de Broglie wavelength $\lambda_e = 2\pi/k$ is directly related to the energy of the emitted photon by: $\hbar^2k^2/2m_e = \hbar\omega$ (this heuristic relation predicts an interference position that agrees well with that obtained from accurate simulations[10,19] for H_2^+). The destructive interference will thus appear in the harmonic spectrum as a clear minimum at a specific harmonic order (harmonic 23 for $\theta = 0$). Recent measurements in aligned CO_2 molecules have given indications of the presence of such a minimum[11,12]. However, those

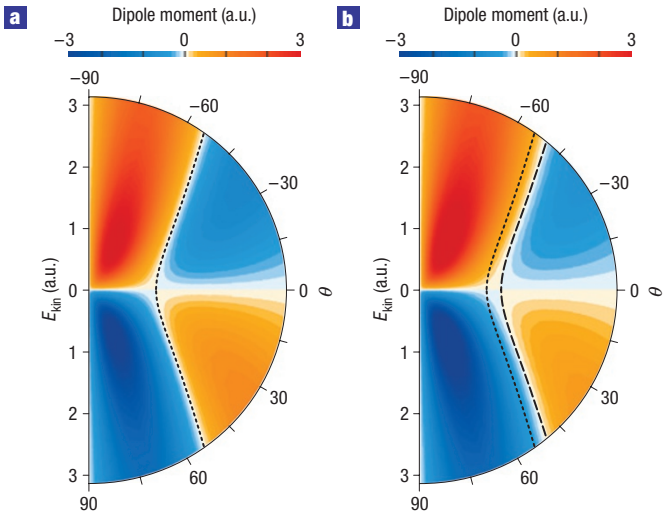

Figure 1 Theoretical dependence of the CO_2 recombination dipole on the angle and energy of the free-electron plane wave. Transition matrix element $\langle \exp[i\mathbf{kr}]|\mathbf{p}|\Psi_0\rangle$ where $\Psi_0 = \Psi_0(\theta, \mathbf{r})$ is the HOMO of CO_2, shown in polar coordinates as a function of the angle θ (°) between the electron wave vector **k** and the molecular axis, and the kinetic energy $k^2/2$ (atomic units) of the electron at recollision. **a**, In Ψ_0, only the *p* orbitals of the oxygen atoms are included. The dipole moment changes sign when the recollision angle θ follows equation (2) with $n = 1$ and $R = 4.3$ a.u. (dotted line). **b**, Total Ψ_0 as obtained from a Hartree–Fock calculation (GAMESS, General Atomic and Molecular Electronic Structure System code). The non-negligible contribution of the d_{xy} (*x* along the internuclear axis) carbon orbital (~7%), and also to a lesser extent of the d_{xy} oxygen orbitals (~2%), shifts the position of the interference to higher energy (equivalent to smaller *R* in equation (2): the prediction for $R = 3.9$ a.u. is shown by the dashed line). The dipole contribution of the d_{xy} carbon orbital obviously does not present any interference. As for the d_{xy} oxygen orbitals, they contribute to the total HOMO as a symmetric combination and thus give rise to a destructive interference following $R\cos\theta = (n-1/2)\lambda_e$. The sum of these different terms leads to the observed deviation. Note that the dipoles in **a** and **b** are real valued.

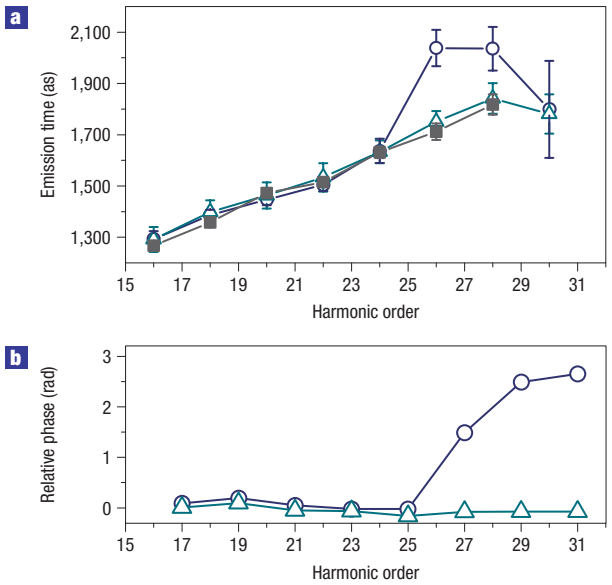

Figure 2 Experimentally measured phase of the harmonic emission from aligned CO_2 molecules. a, Harmonic emission time, that is, frequency derivative of the spectral phase, for molecules aligned parallel (open circles) and perpendicular (open triangles) to the laser polarization, and for krypton atoms (filled squares), under the same generating conditions (intensity of 1.25×10^{14} W cm^{-2}). The error bars indicate the accuracy of the relative phase determination (standard deviation of the phase within the FWHM of the $2\omega_0$ peak in the RABITT trace Fourier transform). Krypton and perpendicularly aligned CO_2 present the same linear dependence of the emission times, corresponding to the free-electron wave-packet dynamics in the continuum[17]. The emission from molecules aligned parallel to the laser exhibits an extra delay between harmonics 25 and 29, corresponding to a rapid increase of the spectral phase. **b**, Difference of spectral phases φ between CO_2 molecules and krypton. Using this reference atom, the subtraction uncovers the phase solely due to the recombination process in the molecule. The phases are obtained from the data shown in **a** by the rectangular integration method. To show the relative phase at harmonic 31, we assumed the emission time at $30\omega_0$ of krypton (that could not be measured owing to the low signal in the cutoff) to be equal to that of perpendicularly aligned CO_2 (measured owing to the slightly higher cutoff). See the Methods section for the choice of the phase zero.

observations rely only on spectral amplitude measurements, and hence could be explained by the interplay between the distribution of the partially aligned molecules and the angular dependence of the harmonic yield[20].

Our analysis is based on the measurements of both amplitude and phase of the harmonic emission from aligned molecules. The spectral phase, although more difficult to measure, contains important information on the interference process. In particular, a phase jump of π is expected at the position of destructive interference[9,18]. Indeed, the sign of the dipole moment in Fig. 1 changes at the amplitude minimum. The harmonic phase is also a crucial element for recovering the symmetry of the molecular orbitals in the tomographic reconstruction procedure[21]. Finally, it gives insight into the ultrafast electron dynamics and enables the reconstruction of the attosecond emission temporal profile.

We have characterized the harmonic emission from non-adiabatically aligned[22] CO_2 molecules (see the Methods section). The 'reconstruction of attosecond beating by interference of two-photon transition' (RABITT) technique[5,17,23] gives access to the relative phases of neighbouring harmonics, and thus to the group delay, also called the emission time:

$$t_e(\omega_{q+1}) := \frac{\partial\varphi}{\partial\omega} \approx \frac{\varphi_{q+2} - \varphi_q}{2\omega_0}.$$

In rare-gas atoms, this emission time varies linearly with the harmonic order in the plateau region, and coincides with the recollision time of the electron trajectories[17]. The resulting frequency chirp of the harmonic emission is a direct signature of the continuum electron dynamics. This is shown in Fig. 2a for krypton, which has a similar ionization potential to CO_2 ($I_p(Kr) = 14.00$ eV, $I_p(CO_2) = 13.77$ eV). Such a reference atom can be used to calibrate the recolliding electron wave packet[21,24]: the first two steps of the harmonic emission process (tunnel ionization and continuum dynamics) are expected to be similar in the two gases (except for the ionization angular dependence; see the Methods section). Indeed, the emission times of the CO_2 molecules aligned perpendicularly to the laser field match very closely with those of Kr (Fig. 2a). However, for parallel alignment, a strong deviation is observed between harmonics 25 and 29. Integrating the difference between the emission times in CO_2 and in Kr gives the phase associated solely with the recombination process (Fig. 2b). It presents a clear jump starting at harmonic 25, close to the prediction of the dipole calculation for the destructive interference. However, there are two remarkable features that are generic to all of our measurements. First, the total phase jump is 2.7 rad in this data set, and not π

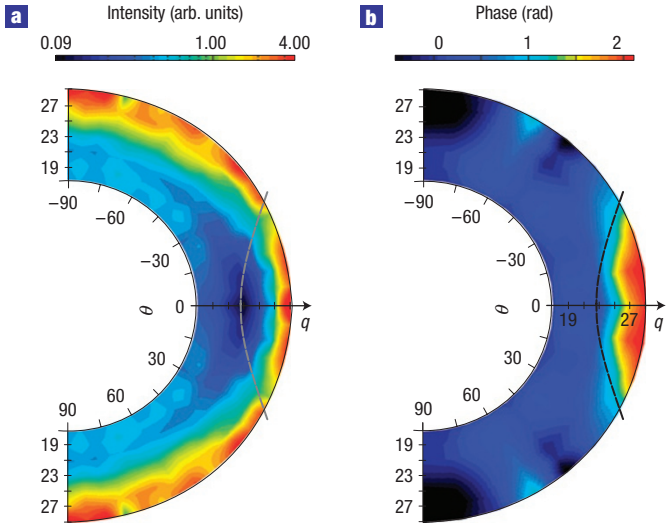

Figure 3 Experimental spectral intensity and phase of the CO_2 harmonic emission normalized by that of Kr. CO_2 harmonic intensity and phase (measured for molecule angles from 90° to 0°) normalized to the krypton data taken under the same experimental conditions (intensity of 0.95×10^{14} W cm^{-2}). To prevent the dispersion effects due to the larger ionization rate of Kr, the corresponding data were taken at lower pressure (25 torr versus 60 torr for CO_2) ensuring good phase-matching conditions. The dashed lines are the same as the one shown in Fig. 1b converted to harmonic order. The relation between the measured data and the recombination dipole moment is given in the Methods section. **a**, Intensity ratio versus alignment angle θ (measured in steps of 5°) and harmonic order q. The ratio is not corrected for the different pressures. A clear intensity minimum is measured around harmonic 23 for $\theta = 0$ that disappears when the molecule is rotated. **b**, Spectral phase difference (as in Fig. 2b), measured in steps of 10°. A phase jump of 2 rad is observed at the same position as the intensity minimum.

(value averaged over eight measurements: 2.0 ± 0.6 rad). Second, this jump is not step-like but is spread over three harmonic orders.

Such deviations cannot be explained by an imperfect experimental alignment: the convolution of the rotational wave-packet angular distribution with the dipole in Fig. 1b (both real-valued functions) would only induce a shift of the interference position but neither a spread nor a reduced value of the phase jump that both correspond to a complex dipole value. Such deviations appeared in early simulations[9,18] in H_2^+ and H_2 single molecules: a reduced phase jump of 2.7 rad spread over five orders was found in H_2^+ and even stronger deviations appeared in H_2. A recent dipole calculation replacing the plane waves in equation (1) by two-centre Coulomb wavefunctions has reproduced this behaviour[19]: the incorporation of the Coulomb binding potential of the atomic centres modifies the prediction of two-centre interference, in particular the shape of the phase jump. Our measured phase jump would thus contain a direct signature of the coulombic distortion of the recolliding electron wave packet, uncovered by the high sensitivity of the quantum interference.

We have carried out careful measurements of the phase jump as a function of the alignment angle (Fig. 3b). It reaches 2 rad for angles below 30° and quickly decreases to 0 with increasing angle. This may correspond to a shift to harmonic orders outside our accessible spectral range, in agreement with the dipole calculation in Fig. 1b. The harmonic amplitudes (Fig. 3a), normalized to those measured in krypton, exhibit a clear minimum around harmonic 23–25 at small angles, which disappears at large angles. The consistency of the amplitude and phase data is excellent and demonstrates a fine control of the quantum interference by turning the molecular axis. Note that the exact position of the interference may change significantly with intensity (phase jump for parallel alignment starting at harmonic 25 in Fig. 2b instead of harmonic 23 in Fig. 3b owing to the larger intensity), as also observed in recent amplitude measurements (Y. Mairesse *et al.*, manuscript in preparation). This extra deviation from the two-point emitter model may explain the different interference positions reported in ref. 11 (harmonic 25) and ref. 12 (harmonic 33).

The temporal characteristics of the quantum interference reveal an unexpected behaviour. With the measured amplitudes and phases, we reconstruct the temporal profile of the extreme-ultraviolet emission[5,17,23], and thus the acceleration of the dipole moment that mirrors the intramolecular electron dynamics. The temporal profile corresponding to orders 17–23 below the phase jump is very similar to that of krypton and does not vary significantly with the alignment angle (Fig. 4a). In contrast, the emission of harmonics 23–29 undergoing the phase jump is delayed in time with respect to krypton by 150 as for small angles and gradually converges to it with increasing angle (Fig. 4b). This delay is due to the quantum interference in the recombination process, and not to the transit time of the electron wave packet between the two oxygen atoms, which is twice as small. The spreading of the phase jump over three harmonic orders shifts the corresponding emission times to larger values (Fig. 2a), resulting in a delayed attosecond emission (Fig. 4b) with a barely modified pulse shape (slightly reduced full-width at half-maximum, FWHM, as compared with perpendicular alignment). This surprising result is a consequence of both the spreading and the occurrence of the quantum interference in the harmonic cutoff. There, the amplitude drops quickly with order, so that the destructive interference between spectral components on either side of the phase jump is not efficient enough to distort the temporal profile. The pulse reconstruction using the experimentally measured phases but assuming equal amplitudes for harmonics 17–29 results in a strong distortion with the expected double peak (Fig. 4c). The strongest distortion of the pulse (double peak with zero amplitude in between) would be obtained for a step-like π phase jump positioned in the middle of a flat spectrum.

The full potential of pulse shaping offered by the measured phase jump can be reached by simultaneously carrying out amplitude shaping. For instance, a clean double pulse could be obtained either using thin filters, or by placing the phase jump in the plateau region of the harmonic spectrum, which should be possible by generating with higher intensity and shorter pulses. By combining amplitude control and phase control (as the position and height of the phase jump depend on molecular structure and orientation), we extend the possibility of coherent quantum control to the extreme-ultraviolet and attosecond domains. For example, coherent transient enhancement of a resonant transition[25] could be carried out if the phase jump of $\sim\pi$ is placed at the transition energy. The below- and above-resonance contributions to the excited state population then interfere constructively.

We have shown how molecular structure and orientation affect the attosecond shape of the total (continuum + bound) electron wave packet during recollision. Further effects could also play a role in shaping the wave packet: (1) interplay of the molecular potential with the strong laser field (Coulomb–laser coupling)[26], (2) Π symmetry of the CO_2 HOMO reflected in the structure of the recolliding electron wave packet[27], (3) ionization dynamics involving many orbitals[27] and in particular orbitals below the HOMO (Y. Mairesse *et al.*, manuscript in preparation), and (4) exchange effects with core electrons[28,29]. At present, the relative importance of these factors is unknown. Our measurements thus

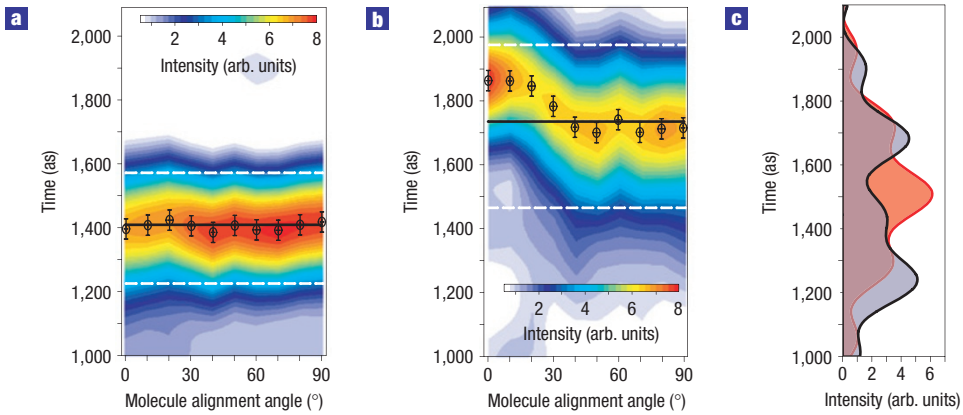

Figure 4 Attosecond dynamics of the harmonic emission from aligned CO_2 molecules. Intensity of a typical attosecond pulse in the generated train mapped as a function of the alignment angle θ and time t, with $t = 0$ at the maximum of the generating field. This dynamics is reconstructed from the spectral information in Fig. 3. Circles give the peak position of the pulse for ten θ values in a series of RABITT scans, and the error bars represent the standard deviation of the emission time of sideband 16, indicating the error in absolute timing of the attosecond pulses[17]. Black and dashed white lines indicate the positions of peak and half-maximum, respectively, of the attosecond pulse generated in krypton under the same experimental conditions. **a**, Using harmonics 17–23, located below the phase jump. The attosecond pulses generated in CO_2 and krypton are the same, with a duration of 320 as FWHM. **b**, Using harmonics 23–29, undergoing the phase jump. For the parallel alignment ($\theta = 0°$), the pulse is shifted by 150 as owing to the phase jump and gradually moves to the same timing as krypton as the molecules are rotated towards the perpendicular alignment. **c**, Time profile for harmonics 17–29 assuming constant spectral amplitudes for $\theta = 0°$ (black) and $\theta = 90°$ (red). Note that we shifted the absolute timing of the pulses in **a–c** with respect to the generating field by +200 as. All emission times in this series including the Kr reference data were measured to be 200 as too low with respect to the data in Fig. 2 and to previous findings[17]. However, the atto-chirp (slope of the emission time versus frequency) in both Figs 2 and 4 was as expected for the intensities used[17]. The small shift of time reference is presumably due to macroscopic effects (dispersion during propagation) and is compensated for here to present the single-atom/molecule response.

provide crucial information to benchmark improved models of the interaction of molecules with strong laser fields.

Our demonstrated control on the attosecond timescale provides a way to generalize the use of the continuum electron wave packet as a probe of molecular systems, in particular for accurate *ab initio* tomographic imaging of molecular orbitals. The extreme-ultraviolet spectral phase could also be used to probe coulombic recolliding electron wave packets. Finally, the control of the attosecond emission is a further step towards the extreme-ultraviolet pulse shaping that will open a new class of experiments, such as extreme-ultraviolet coherent control of atomic and molecular systems.

METHODS

We used the Laser Ultra-Court Accordable (LUCA) laser facility, which delivers to our experiment infrared pulses of 50 fs duration and up to 30 mJ in energy. A supersonic gas jet of CO_2, cooled in expansion to a rotational temperature of about 90 K, provides the molecular sample. An aligning laser pulse focused up to 5×10^{13} W cm^{-2} with a lens of 1 m focal length creates a rotational wave packet in the medium[22]. This wave packet periodically rephases, giving at the revival times a strong molecular alignment along the polarization direction (angular distribution of the rotational wave packet confined in a cone angle of ~20°). At the half revival time (equal to half the rotational period of the molecule), a second, more intense laser pulse of approximately 1×10^{14} W cm^{-2} generates high harmonics from the aligned molecules. A micrometric motorized translation stage is used to control the delay, and the angle between the axis of molecular alignment and the polarization of the generating beam is monitored by a motorized half-wave plate inserted in the aligning beam. To implement the RABITT technique, we need a third, weaker pulse of intensity about 10^{11} W cm^{-2}, the synchronization of which with the generating pulse is controlled by a piezoelectric translation stage. After harmonic generation, a diaphragm blocks the aligning and generating beams. A broadband toroidal mirror under grazing incidence focuses the harmonics and dressing beam in a detecting neon jet placed in the source volume of a magnetic-bottle electron spectrometer (see ref. 17, Fig. 2 for the phase measurement part of the set-up).

This demanding set-up requires precise alignment of three laser beams (aligning, generating and dressing), the intensities, delays and polarization of which should be controlled independently. In particular, the interferometric stability needed by the RABITT measurements must be preserved for more than 1.5 h to carry out the acquisition of the data shown in Fig. 3.

The RABITT technique measures the derivative of the harmonic phase, not the phase itself. To get a phase reference for Figs 2b and 3b, we assume that the phase of harmonic 15 generated in CO_2: (1) does not vary with angle and (2) for convenience, is the same as the one in Kr. The first assumption is supported by recent interferometric experiments (Y. Mairesse *et al.*, manuscript in preparation) demonstrating a very weak angular dependence of the phase of low harmonics in CO_2.

Within the plane-wave approximation, the transition dipole moment $d_{CO_2}(\omega, \theta)$ between a continuum state and the CO_2 HOMO can be directly related to the harmonic intensity ratio $S_{CO_2}(\omega, \theta)/S_{Kr}(\omega)$ and phase difference $\varphi_{CO_2}(\omega, \theta) - \varphi_{Kr}(\omega)$ measured in CO_2 and the krypton reference gas using[21]:

$$d_{CO_2}(\omega, \theta) = \langle \Psi_c | \mathbf{p} | \Psi_{CO_2} \rangle = \sqrt{\frac{P_{Kr}}{P_{CO_2}(\theta)}} \sqrt{\frac{S_{CO_2}(\omega, \theta)}{S_{Kr}(\omega)}}$$

$$\times \exp[i(\varphi_{CO_2}(\omega, \theta) - \varphi_{Kr}(\omega))] \langle \Psi_c | \mathbf{p} | \Psi_{Kr} \rangle,$$

where Ψ_{CO_2} is the CO_2 HOMO wavefunction, Ψ_{Kr} is the $4p$ orbital of krypton, Ψ_c is a plane wave $\exp[i\mathbf{k}(\omega)\mathbf{r}]$ propagating along the laser polarization direction, P_{CO_2} is the angle-dependent ionization yield of CO_2 and P_{Kr} is the ionization yield of Kr. As the Kr dipole is real valued and presents a smooth behaviour, it does not significantly modify the structures observed in Fig. 3 that can thus be attributed to the CO_2 dipole. Note finally that the above formula does not apply at $\theta = 0$ and 90° where the ionization is suppressed in CO_2 owing to the HOMO symmetry.

Received 21 December 2007; accepted 3 April 2008; published 4 May 2008.

References

1. Drescher, M. *et al.* Time-resolved atomic inner-shell spectroscopy. *Nature* **419**, 803–807 (2002).
2. Remetter, T. *et al.* Attosecond electron wave packet interferometry. *Nature Phys.* **2**, 323–326 (2006).
3. Baker, S. *et al.* Probing proton dynamics in molecules on an attosecond time scale. *Science* **312**, 424–427 (2006).

4. Cavallieri, A. *et al.* Attosecond spectroscopy in condensed matter. *Nature* **449**, 1029–1032 (2007).
5. Paul, P. M. *et al.* Observation of a train of attosecond pulses from high harmonic generation. *Science* **292**, 1689–1692 (2001).
6. Hentschel, M. *et al.* Attosecond metrology. *Nature* **414**, 509–513 (2001).
7. Sola, I. *et al.* Controlling attosecond electron dynamics by phase-stabilized polarization gating. *Nature Phys.* **2**, 319–322 (2006).
8. Pfeifer, T. *et al.* Single attosecond pulse generation in the multicycle-driver regime by adding a weak second-harmonic field. *Opt. Lett.* **31**, 975–977 (2005).
9. Lein, M., Velotta, R., Marangos, J. P. & Knight, P. L. Role of the intramolecular phase in high-harmonic generation. *Phys. Rev. Lett.* **88**, 183903 (2002).
10. Lagmago Kamta, G. & Bandrauk, A. D. Three-dimensional time-profile analysis of high-order harmonic generation in molecules: Nuclear interferences in H_2^+. *Phys. Rev. A* **71**, 053407 (2005).
11. Kanai, T., Minemoto, S. & Sakai, H. Quantum interference during high-order harmonic generation from aligned molecules. *Nature* **435**, 470–474 (2005).
12. Vozzi, C. *et al.* Controlling two-center interference in molecular high harmonic generation. *Phys. Rev. Lett.* **95**, 153902 (2005).
13. McPherson, A. *et al.* Studies of multiphoton production of vacuum-ultraviolet radiation in the rare gases. *J. Opt. Soc. Am. B* **4**, 595–601 (1987).
14. Ferray, M. *et al.* Multiple-harmonic conversion of 1064 nm radiation in rare gases. *J. Phys. B* **21**, L31–L35 (1988).
15. Corkum, P. B. Plasma perspective on strong field multiphoton ionization. *Phys. Rev. Lett.* **71**, 1994–1997 (1993).
16. Schafer, K. J., Yang, B., DiMauro, L. F. & Kulander, K. C. Above threshold ionization beyond the high harmonic cutoff. *Phys. Rev. Lett.* **70**, 1599–1602 (1993).
17. Mairesse, Y. *et al.* Attosecond synchronization of high-harmonic soft X-rays. *Science* **302**, 1540–1543 (2003).
18. Lein, M., Hay, N., Velotta, R., Marangos, J. P. & Knight, P. L. Interference effects in high-order harmonic generation with molecules. *Phys. Rev. A* **66**, 023805 (2002).
19. Ciappina, M. F., Chirila, C. C. & Lein, M. Influence of Coulomb continuum wave functions in the description of high-order harmonic generation with H_2^+. *Phys. Rev. A* **75**, 043405 (2007).
20. Le, A.-T., Tong, X.-M. & Lin, C. D. Evidence of two-center interference in high-order harmonic generation from CO_2. *Phys. Rev. A* **73**, 041402 (2006).
21. Itatani, J. *et al.* Tomographic imaging of molecular orbitals. *Nature* **432**, 867–871 (2004).
22. Rosca-Pruna, F. & Vrakking, M. Experimental observation of revival structures in picosecond laser-induced alignment of I_2. *Phys. Rev. Lett.* **87**, 153902 (2001).
23. Wabnitz, H. *et al.* Generation of attosecond pulses in molecular nitrogen. *Eur. Phys. J. D* **40**, 305–311 (2006).
24. Levesque, J., Zeidler, D., Marangos, J. P., Corkum, P. B. & Villeneuve, D. M. High harmonic generation and the role of atomic orbital wave functions. *Phys. Rev. Lett.* **98**, 183903 (2007).
25. Dudovich, N., Oron, D. & Silberberg, Y. Coherent transient enhancement of optically induced resonant transitions. *Phys. Rev. Lett.* **88**, 123004 (2002).
26. Smirnova, O., Mouritzen, A. S., Patchkovskii, S. & Ivanov, M. Yu. Coulomb–laser coupling in laser-assisted photoionization and molecular tomography. *J. Phys. B* **40**, F197–F206 (2007).
27. Xie, X. *et al.* Subcycle dynamics in the laser ionization of molecules. *Phys. Rev. A* **76**, 023426 (2007).
28. Patchkovskii, S., Zhao, Z., Brabec, T. & Villeneuve, D. M. High harmonic generation and molecular orbital tomography in multielectron systems: Beyond the single active electron approximation. *Phys. Rev. Lett.* **97**, 123003 (2006).
29. Zhao, Z., Yuan, J. & Brabec, T. Multielectron signatures in the polarization of high-order harmonic radiation. *Phys. Rev. A* **76**, 031404 (2007).

Acknowledgements

We acknowledge financial support from the EU-FP6 XTRA (MRTN-CT-2003-505138) and LASERLAB (RII3-CT-2003-506350) programmes, the ANR Attoscience and the Engineering and Physical Sciences Research Council (UK) (GR/S22424/01).

Author contributions

P.S. with B.C., H.M. and P.M. planned the project. W.B., H.M., P.B., P.M., B.C. and P.S. designed and installed the experiment. W.B. and S.H., with assistance from H.M., P.B., G.W., M.S., L.J.F., P.M. and P.S. carried out the measurements. W.B., S.H., H.M. and P.S. analysed the data. R.T., J.C. and A.M. carried out the dipole simulations. All authors discussed the results and contributed to the final manuscript. W.B. and S.H. contributed equally to this work.

Author information

Reprints and permission information is available online at http://npg.nature.com/reprintsandpermissions. Correspondence and requests for materials should be addressed to P.S.